LA-UR- 10-05417

Approved for public release;
distribution is unlimited.

Title:	A semi-automatic method for extracting thin line structures in images as rooted tree network
Author(s):	Jacopo Grazzini Scott Dillard Pierre Soille
Intended for:	International Symposium on Visual Computing

Los Alamos
NATIONAL LABORATORY
EST. 1943

Form 836 (7/06)

A semi-automatic method for extracting thin line structures in images as rooted tree network

No Author Given

No Institute Given

Abstract. This paper addresses the problem of semi-automatic extraction of line networks in digital images - *e.g.*, road or hydrographic networks in satellite images, blood vessels in medical images. robust, For that purpose, we improve a generic method derived from morphological and hydrological concepts and consisting in minimum cost path estimation and flow simulation. While this approach fully exploits the local contrast and shape of the network, as well as its arborescent nature, we further incorporate local directional information about the structures in the image. Namely, an appropriate anisotropic metric is designed by using both the characteristic features of the target network and the eigendecomposition of the gradient structure tensor of the image. Following, the geodesic propagation from a given seed with this metric is combined with hydrological operators for overland flow simulation to extract the line network. The algorithm is demonstrated for the extraction of blood vessels in a retina image and of a river network in a satellite image.

1 Introduction

The detection of line networks - *aka* thin nets or curvilinear structures - is a common low-level task in computer vision as they are usually related to the presence of salient features in images [1, 2]. Indeed, they are found in numerous applications fields and have received considerable attention, in particular in medical imaging and remote sensing. Typical examples are provided by the identification of roads from aerial or satellite images, which involves the detection and following of line segments and/or the detection of the road edges [3]; other common applications regard the extraction of railroads, trails and rivers [4, 5]. Many techniques have been proposed, which can be broadly classified as semi-automatic approaches and automatic approaches. The main criterion for the classification is whether the approach requires human intervention [6]. In semi-automatic approaches, an operator provides information such as starting points or starting directions, which provide critical assistance in tracking. Without human intervention, an approach is considered automatic [7].

Because local pixel attributes are intrinsically ambiguous - *i.e.*, pixels belonging to the same object (*e.g.*, a river, a road, a vessel) can vary considerably while pixels belonging to different objects may have similar values -, approaches based on such attributes only, such as various thresholding methods and classification techniques, have only limited success [8, 9]. Besides, due to the noise

sensitivity, asymmetry of the contrast at the both sides of the edges, and the difficulty of obtaining precise edge directions, edge-based methods are inadequate for extracting linear networks [10]. Instead, the extraction of line networks is often based on a two steps approach. The first one typically leads to an initial detection of the desired network avoiding false positive detections but containing gaps. It is usually performed through local filtering, segmentation and/or classification of the input image [3, 4] and exploits knowledge about the spatial and spectral properties of the target network [11], sometimes also models of it [12]. The second step consists in post-processing the obtained output in order to bridge the gaps, and often uses tracking-based or perceptual grouping techniques. In this context, recent and advanced techniques have been successfully developped for the detection of tubular structures, like blood vessels, in medical images [12, 11] or the extraction of linear features, like river networks, in large scale remotely sensed images [4]. In particular, the authors of [4] propose to exploit the geometrical and topological characteristics of the rivers and their tributaries in order to reconstruct hydrographic networks in satellite optical images. For that purpose, their approach combines - likewise the watershed based segmentation - concepts arising from mathematical morphology and hydrology. Similarly to [1], it performs the robust extraction of line networks by applying minimum cost path techniques searching for the path which contains most line evidence. However, it differs from [1] as it fully exploits the fact that the hydrographic network has a tree-like structure (with a root) and the knowledge of arborescent networks. It further uses Contributing Drainage Areas (CDA) computed on a potential function defined from the image characteristics as a proxy to evidence the presence of a network (the higher the value of the CDA, the higher the probability of belonging to a network). By construction, the method leads to connected networks. In addition, it can be easily adapted for the extraction of other arborescent networks. Namely, the generic methodology for extracting line networks from a single image can be summarised as follows:

(i) define the reference set as the set of *outlets* and *seeds* of the target network, *e.g.* pixels belonging most surely to it,
(ii) define the *potential stretches* (referred to as *geodesic mask* in [4]) as the image with enhanced linear features, *e.g.* computed using relevant spectral and spatial properties,
(iii) generate the so-called pseudo Digital Elevation Model (DEM) by estimating the shortest paths originating from the seed and 'constrained' by the enhanced image,
(iv) calculate the local flow directions of the pseudo DEM and its CDA,
(v) trim the resulting space filling network so as to obtain a network matching the target network.

In this paper, we adopt the same methodology, but improve its major steps. First, we derive a new rank-based operator for qualifying the potential stretches in step *(ii)*. Second, we incorporate directional information about the local structures in the image through the computation of the gradient structure tensor (GST) when reconstructing the pseudo DEM in step *(iii)*, and we use a Fast

Marching Method (FMM) instead of the Dijsktra's algorithm, for that purpose. Third, we refine the estimation of the CDA in step *(iv)* using an improved nondispersive flow estimation technique. Last, we perform a additional post-filtering that enables to fill the gaps and retrieve missing branches of the network:

(vi) compute the shortest paths linking the endpoints (leaves) of the previously detected network and check for possible 'shortcuts'.

Therefore, our approach makes use of both local and global characteristics of line networks: locally, those networks are modeled as elongated regions with a smooth spectral signature in the image and a maximum width; globally, they are structured like a tree. It provides the framework for semi-automatic and robust extraction of line networks in various types of images.

The rest of the paper is organised as follows. Sec. 2 presents the assumptions made for the network, and therefore the image, with regards to the image resolution in particular. Steps *(i)* to *(vi)* are successively presented in sections 3 to 7 *resp.* Results are illustrated on a retina image already used in [4] and compared with [4]. A conclusion to this work is presented in Sec. 8.

2 Image characteristics and networks properties

Our approach is based on the intrinsic properties that a line network is made of elongated structures composed with groups of 'similar' pixels[1]. The similarity is defined in the overall shape of the region they belong to, the spectrum they share, and the geometric property of the region. Therefore, we assume images to satisfy the following two general assumptions which are the minimum conditions for a line network to be identifiable:

- visual constraint: most pixels compopsing the network have similar (uniform, possibly textured) spectrum that is distinguishable from most of the surrounding areas; this does not require the network to have single color or constant intensity, it mainly requires the network to look visually different from surrounding objects in most parts (good contrast);
- geometric constraint: a line is a region that isrelatively long and narrow, compared with other objects in the image; it does not require a smooth edge, only the overall shape to be a long narrow strip whose width should not change significantly.

For a given resolution, a linear network may appear as having a width of approximately a single pixel, or multiple pixels, depending on the object's (road, river, vessels, ...) actual width. Differences in how single and multiple pixel width linear features are manifest in digital image and imposes an important control on the techniques used to extract the features. Still, we consider that the conditions above are usually met by most low- to mid-resolution images, where the

[1] This is in fact in agreement with Gestalt theory stating that elements tend to be perceptually grouped if they are close to each other (proximity), similar to one another (similarity) or form a smooth and continuous curve (good continuation).

network is typically $\rho < 10$ pixels-width. Thin structures typically consist of groups of spectrally similar pixels oriented along a narrow line, whereas other structures tend to have a more compact and isotropic shape [1]. For instance, in satellite optical images, most roads consist of straight line segments of dark pixels connected with smooth curves, normally circular arcs and their width typically ranges from 1-pixel to 7-pixels: therefore, extraction of road networks in that case is equivalent to detection of lines or strong curvilinear structures [13]. Consider now Fig. 1, bottom. Similarly, rivers in optical images are detectable by a human operator owing to their shape and relative contrast since they appear as dark networks of thin lines. Blood vessels are also identified as long linear segments of (almost constant) bright pixels with longer segments having more confidence of being part of the vessel network than segments with short length.

3 Seed and outlets selection

Both steps *(i)* and *(ii)* make the algorithm semi-automatic, as they both require the intervention of a user with knowledge about the target network. Indeed, it is required for an external operator to provide a set of initial seed point(s) on the network. This set can be entered manually by an expert - a physician locating a pixel of interest in medical images - or derived from an external source of information - the location of a road intersection in a satellite image given by its coordinates in a geographic information system. This approach can be extended to a fully-automatic one by using the outputs of a previous detection [14] or by extracting the features that are relatively easier to identify such as major lines [15]. Still, the reason for keeping the method semi-automatic in our design is a balance between reliability and efficiency. This way, we want to ensure that the line network passes through the reference set, which is crucial for its construction.

4 Morphological thin lines enhancement

Next, the geodesic mask (See Sec. 1) needs to be generated. This preprocessing step aims in fact at providing a potential image identifying key pixels in the image that are likely components of the network. A potential value can be either a fuzzy degree, a probability, or a value resulting from any other prior detector, *e.g.* line extractor filters [13]. We can derive from such a filter a greylevel image corresponding to the magnitude of their response, which gives us a potential image to work with. In order to generate as many line network candidates as possible, we propose to use here a morphological filter for enhancing lines.

The primary features classically used for the identification of potential lines are spectral features. For instance, band combinations of multispectral satellite images defining either a water index or a vegetation index can be used to identify river or road networks [5, 3]. In medical images, tubular shapes, like vessels, are usually located in brighter or darker areas [12, 16]. The other features characterising a line network are length-width contextual features that measure the dimensions and directionality of connected pixels [17, 1, 4], see previous Sec. In

order to filter out interference as much as possible, a minimum region width can be imposed. Following, the fact that water has low reflectance values in satellite images is used in [4], while the knowledge about the shape, size, and local contrast of river stretches is also translated into a series of morphological operations [17]. This way, a geodesic mask where potential river pixels are set to low values is obtained. The extraction of potential (dark) network pixels is achieved by initially suppressing these networks with a parametric closing - or rank-min closing owing to its representation in terms of a rank filter [18] - by a 2D shaped structuring element (SE), followed by a top-hat by the difference between the closing and the input image, called top-hat by closing [4]. Instead, we apply a sequence of directional rank-min closing $\{\phi_{k,\lambda,\theta}\}_{k,\theta}$, with 1D SE's of increasing lenght k, different orientations θ but constant rank λ. Top-hat by closing operators are thus performed at different scales and orientations (*e.g.* 3 orientations), and then combined by setting the pixels in the image I to the number of positive responses they produce at any orientation in the different scales:

$$\mathrm{F} = \sum_{k=k_1}^{k_n} \sup_{\theta \in \{0,\pi/4,\pi/2\}} \{T_{[0,0]}(\phi_{k,\lambda,\theta}(I) - I)\} \in [1, n] \tag{1}$$

with $T(\cdot)$ the threshold operator, λ a constant and where the initial lenght k_1 slightly exceeds the width of the target network. F quantifies the min and max lengths of the linear structures consisting of spectrally similar pixels (Fig. 1, 3rd column). It also leads to many false positive detections, but they are coped by the subsequent steps provided that higher rate of detection are obtained for actual stretches. Thus, all pixels which have a non null value F are considered as potentially belonging to the network. The geodesic mask W is formed by keeping these pixels to that value, while all the other pixels retain their original value in I incremented by n (Fig. 1, 4th column):

$$\mathrm{W} = (I + n) \cdot T_{[0,0]}(n - \mathrm{F}) + (n - \mathrm{F}) \cdot T_{[0,n-1]}(n - \mathrm{F})\,. \tag{2}$$

This operator enables the prior enhancement of potential linear and thin stretches that could not be detected solely on the basis of their spectral values. This way, features are represented with (the complement of) a confidence value that the line element is part of the network: a low potential W-value assigned to a pixel means that it is very likely to belong to the network; on the contrary, a high potential W-value means that this pixel may not belong to the network. Yet, the network is still noisy and incomplete (both false and positive alarms) and disconnected (see Fig. 1), but the proposed scheme does not require to be precise. It also does not exclude the use of additional visual and geometrical information, when available, to further improve the quality of the line extraction. In particular, the information from already extracted lines can be used to simplify the process of identifying the components of the network that are less visible or heavily impacted by surrounding objects.

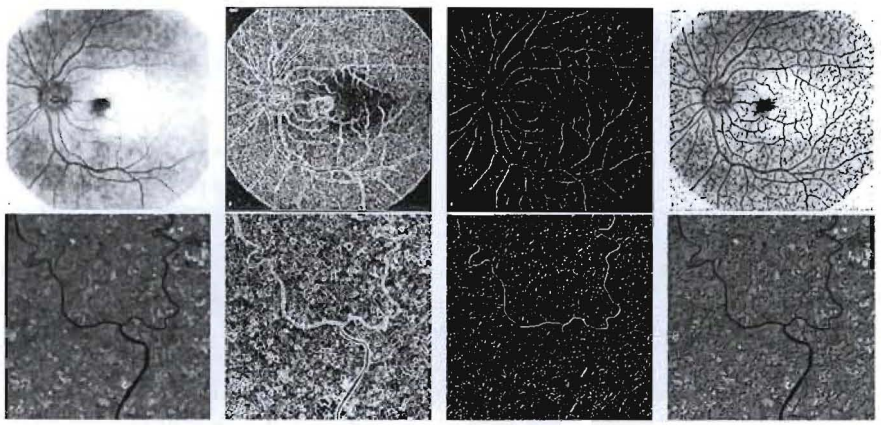

Fig. 1. Examples of line networks typically observed - blood vessels in a eye retina image (top), river in a satellite image (bottom) - and the derived functions used for building the anisotropic metric of Eq. (5). From left to right: original image, its GST norm N (the darker a pixel, the lower its norm), the function F (the brighter a pixel, the longer the lines passing through it) computed for $k_1 = 5, k_n = 30$ and $\lambda = 3$ in both cases (networks of similar size) and the resulting geodesic mask W enhancing dark elongated features.

5 Network propagation

The reconstruction of the network from its seed through the linking of line pisels is an ill-defined problem since the curves are likely to contain gaps and branches. More attractive is the 'edge tracker', which is based on the idea of following the network in the image. More specifically, starting from the seed pixel, the next point to be linked to the network is searched for. The approaches may involve a heuristic methods [13] or minimal path searching [1]. Following [4], this latter approach is used, where the shortest path(s) originating from the seed and containing most line evidence is extracted.

Indeed, step *(iii)* implements geodesic transforms applied to the geodesic mask and enables to mimic a pseudo DEM representing the propagation from the seed through the network. Geodesic transforms are classical operators in image analysis [19, 16], as a large class of problems can be formulated as the extraction of shortest - or geodesic - path(s) for a given discrete or continuous metric [20, 2, 16]. In the continuous setting, it is classical to equip the image domain Ω with a positive metric $\Phi(s)\,ds$ and to define the *weighted length* τ_Φ of a path $\gamma : [0,1] \to \Omega$ as [16]:

$$\tau_\Phi(\gamma) = \int_\gamma \Phi(s)\,ds = \int_0^1 |\gamma'(t)|\,\Phi(\gamma(t))\,dt \tag{3}$$

the isotropic eikonal equation, the anisotropic FMM involves the sweeping of the image embedded in a discretisation grid by progressively propagating the front, but does not resort to any anisotropy related parameter to constrain this propagation, Compared to Dijkstra algorithm [4], the FMM computes geodesics with the same computational complexity but more accurate estimation. When computing geodesic paths with Eq.(4), $f^{\pm}$ define the strenght of the propagation in respective directions $e_{\pm}$. α defines the relative influence given to the geodesic mask $w.r.t$ the orientation for the reconstruction of the network, depending on the confidence in their estimation. Therefore, since $f^{+} \leq f^{-}$, a path γ has a shorter local length if its speed $\gamma'(t)$ is collinear to e_{-} [16]. This way, the front propagates faster along the direction of the potential network, *i.e.* the endpoints of the line structures are allowed to "grow" in the general direction of the line. The propagation is 'forced' to follow the low values of the geodesic mask W in that direction through the term $(1+W)^{-1}$ inherited from [4]. The additional term $N/\max_{\Omega}\{N\}$ in Eq.(5) further constrains the propagation to the centerline of the network (low N-values), and is therefore valid for wide line networks ($\rho > 3$ pixels). For narrow networks ($\rho < 3$ pixels, centerline pixels have then high N-values), the tensor should be simply modified as follows: $f^{+} = (N/\max_{\Omega}\{N\}) \cdot (1+W)^{-\alpha}$. The main consequence of such potential images is that, independently of the input image resolution, centerline pixels are identified to represent the network. Note moreover, that as line segments are identified and added to the line network, the endpoints of the line segments could be possibly used to further propagate the network.

6 Network extraction and trimming

The pseudo DEM can be viewed as a height map image where the intensity value of a pixel represents its elevation and whose 'valleys' match the target network. In order to extract these valleys, the best available method relies on the simulation of a nondispersive flow of water on digitised topographic surfaces [5, 23]. The flow direction of a pixel is defined for each pixel as the direction of the 8-neighbour producing the steepest slope. In this sense, each point of the terrain belongs to the network of streams [4]. However, the classical extraction of nondispersive flow paths suffer serious uncertainty because of the lack of variability, *i.e.* only 8 allowed flow directions. Instead, we use here the improved estimation technique based on global search of [24], which has the advantage of reducing this uncertainty (Fig. 2 middle). This approach also assumes that all spurious minima have been filtered out beforehand and that every point, except for the seed, have at least one neighbour with a lower elevation than the considered point [23, 4]. Following, CDA are calculated by simulating the flow of water on the pseudo DEM using the flow directions for the computation of the number of pixels located upstream of each point of the DEM. See [4] and references therein for further discussion. Actual line network pixels are then identified as as the downstream of all pixels whose CDA exceeds some value. Their extraction can achieved by adaptive thresholding using a priori knowledge

(*aka geodesic time* [4] or *weighted distance* [19]). The geodesic distance between two pixels $\mathbf{x}, \mathbf{y} \in \Omega$ is defined as the minimal lenght of all the paths joining them: $\tau_\gamma(\mathbf{x}, \mathbf{y}) = \min\{\tau_\Phi(\gamma) \mid \gamma(0) = \mathbf{x}, \gamma(1) = \mathbf{y}\}$ and is reached over geodesic paths. In Eq.(3), Φ defines on each pixel a weight that penalises the path γ passing through it, *i.e.* it gives the *potential function* for moving along γ [19, 16]. In particular in [4], this function is set to the geodesic mask so that the derived metric Φ is the Euclidian distance weighted by W. Since potential line pixels are set to low values in W, the propagation goes faster through those pixels and the geodesic paths follow the network lines as desired. This way, the local contrast and shape of the network, as well as its arborescent nature, are fully exploited for its reconstruction. Still, the propagation does not take into account directional information regarding the network. Namely, the gradient edge magnitude is however not enough for capturing thin structures, important - so far neglected - additional information is the orientation of the image gradients.

Ideally, one should incorporate the local direction of salient image structures into the estimation of the geodesic paths, so that they are further constrained to follow the line network. Anisotropic propagation is made possible by defining a local Riemannian metric Φ associated with a tensor field $\mathbf{T}$ - defined as a positive symmetric matrix - that allows to measure a geodesic path γ as follows [16]:

$$\tau(\gamma) = \int_0^1 \sqrt{\gamma'(t)^T \mathbf{T}(\gamma(t))\gamma'(t)}\, dt\,. \tag{4}$$

The difficult task is the design of the tensor T so that meaningful geodesics are derived. In this context, it seems natural to first consider the GST, which is a local measure of the directional signal variations based upon the gradient, in order to retrieve the local geometry and orientation of the image I. The classical method for estimating the GST consists in computing locally the matrix $\mathbf{S} = K_\rho \star (\nabla I_\sigma \nabla I_\sigma^T)$, where $\star$ is the element-wise convolution operation, ∇I_σ is the gradient of the image I pre-smoothed by a Gaussian with scale σ, and K_ρ is an analogous smoothing kernel of scale ρ [21]. $\mathbf{S}$ enables to extract both the local direction of edges and textural patterns. The eigenvectors e_+, e_- of $\mathbf{S}$ are the directions of maximal and minimal variations of I at a given point, while the corresponding eigenvalues $\lambda_+ \geq \lambda_-$ give the respective rates of change. These values together discriminate different local geometries [21]. The corresponding eigenvectors e_+, e_- are the directions of maximal and minimal changes. The information contained in the eigen-decomposition $\lambda_\pm$ and $e_\pm$ of $\mathbf{S}$ is then used to build the tensor field $\mathbf{T} = f^+ e_+ e_+^T + f^- e_- e_-^T$ as follows:

$$\begin{cases} f^+ = (1 - N/max_\Omega\{N\}) \cdot (1 + W)^{-\alpha} \\ f^- = (1 + W)^{-1} \end{cases} \tag{5}$$

with W the enhanced image defined in Sec. 4, $N = (\lambda_+ - \lambda_-)$ approximating the norm of the image gradient, and $\alpha \geq 1$ controling the anisotropy (here we set $\alpha = 2$). In order to efficiently compute the anisotropic geodesic paths, a Fast Marching Method (FMM) developed for computing geodesic distances with generic Riemannian metrics is employed [22]. Like classical FMM [20, 16] solving

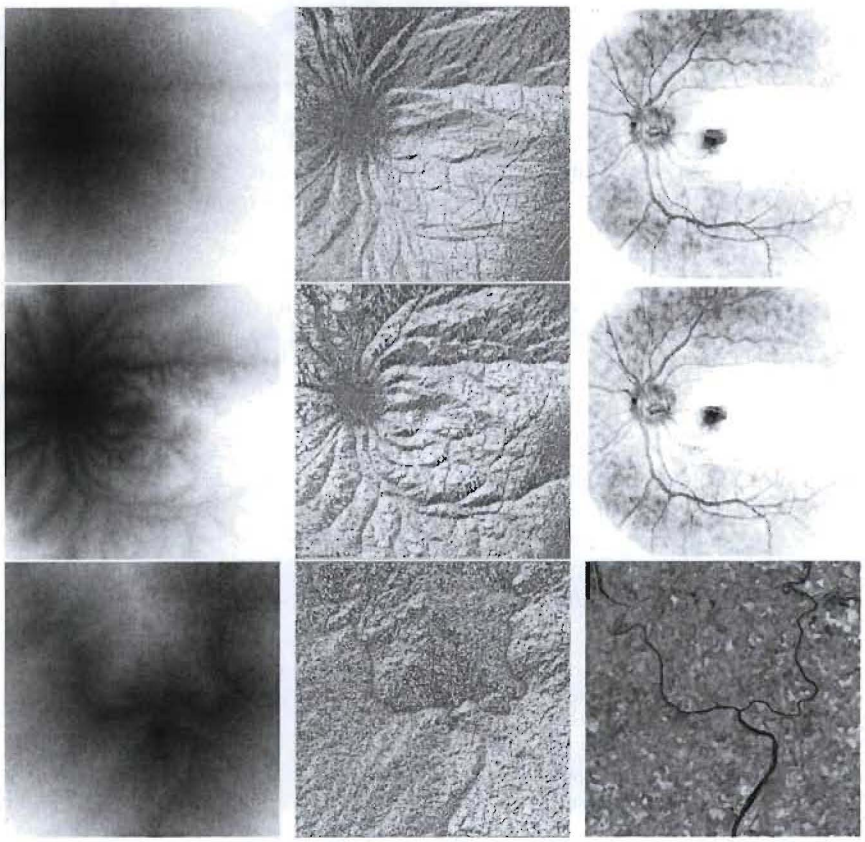

Fig. 2. Network extraction in the images of Fig. 1. Results of the approach of [4] (top) and current approach (middle) are output for the vessel image. Output of the current approach is displayed for the river image. From left to right: pseudo DEM's generated as the geodesic distance (the darker a pixel, the lower its distance to the seed) estimated from a seed manually placed (in the center of the retina or at the crossroad *resp.*), color representation of the corresponding flow directions (value in [1,8] indicated the direction in a 8-neighbourhood) and extracted networks.

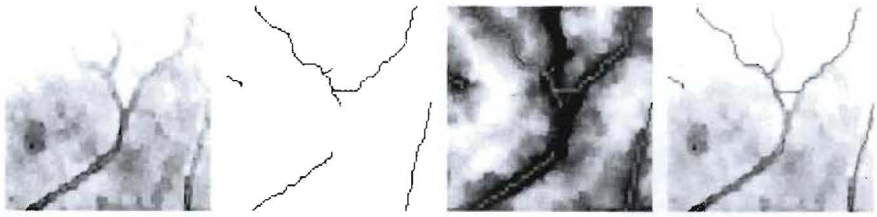

Fig. 3. Filling gaps occuring in the network: an excerpt for the procedure applied on the retina image is shown. From left to right: network output by adaptive threholding of the pseudo DEM (notice an inherent drawback of shortest paths based approaches: the path joining two branches takes a shortcut), leaves extracted through morphological procedures (displayed in red), new pseudo DEM estimated from the set of all leaves found in the image and estimated geodesic paths (shortcuts) occuring between pairs of closest leaves. This gap filling procedure has to be iterated till all (pairs of) leaves have been explored. The two leaves 'facing' each other are linked very early. The leave on the left of this excerpt is not linked to any other leave in the image: it is a real terminal leave while the one on the top of the image is reached by another leave (outside this excerpt) through the displayed shortcut.

or further transformations of the input image [23]. Here, Strahler branching ratio, which uses global properties on ordering and relationships between branches, is chosen for filtering, but other topological indices can be used [25]. Strahler indice measures the symmetry and elongation of the branching structure, it is calculated by ordering all the edges within a given tree.

7 Filling the gaps

It can be seen in Fig. 2 that the estimated anisotropic geodesic front (middle) 'tracks' well the main blood vessels of the network, without spreading in smaller branches due to noisy artefacts in the image. The flow estimation reduces the uncertainty residing in local searches and produces more natural flow patterns (middle). In comparison to [4], the resulting extracted network (bottom) better deals with interruptions - *e.g.* a bridge on a road - and bifurcations - *e.g.* anastomosis of blood vessels - in the network, as it takes into account the orientation of the structures present in the image to 'prolong' them. However, some gaps are still present in the extracted network. Indeed, [1] identifies several errors general for the extraction of line networks - like the presence of spurious line structures in the image which may generate distortions - errors specific for minimum cost path based methods. In particular, specific for the algorithm is *(a)* the inability to trace more than one line between connections: in general, only one path between two pixels is of minimum cost, any other path connecting the same pixels will be removed, and *(b)* the sensitivity to shortcuts: when a shorter path exists in the neighborhood of the traced path, the algorithm tends to take

a shortcut via this path. Under some severe noise, part of the network may also be disqualified as valid segments and hence missed, leaving some major gaps.

These issues can be partially solved by a post-processing based on the propagation from the endpoints (leaves) of the primary detected network, completing the network extraction. Remaining small 'gaps' are eliminated using the property of line networks, that most pixels can be reached from all other points with minimum detour. For each endpoint, the optimal path within the geodesic mask to its closest endpoint is estimated and compared to the connection between them along the network. If the estimated path does not belong to the primary network (hence, it is shorter), the new connection is inserted (*i.e.* a gap is closed) into the network (see Fig. 3). This post-processing has to be repeated until no more new endpoints can be generated. The result of this global completion step is the final line network.

8 Conclusion

Similar to the approach of [4] it is derived from, the proposed method for extracting line networks lies in the idea - common to watershed segmentation - of combining the geodesics computed for an appropriate metric built from the network characteristic in the image with hydrological concepts developped for overland flow simulations. This approach exploits both local and global information based on spatial and spectral properties of the line network of interest. The local contrast, shape and size of the network, but also its direction as well as its arborescent nature, are exploited for its extraction from the anisotropic geodesic front through the introduction of an approapriate anisotropic metric. This way, topological changes (obstructions and bifurcations) can be handled, and a priori domain knowledge (*e.g.*, structural constraints) can be further incorporated into the evolution process. If necessary, additional physical information about the network and/or the image can still be used to better constrain the generation of the pseudo DEM. Besides, the extraction of the network requires minimal operator assistance as it is able to extract the network from a single seed point, and can be easily made automatic. This technique can be also refined by combining the outputs for multiple seeds when such information is available.

References

1. Geusebroek, J., Smeulders, A., Geerts, H.: A minimum cost approach for segmenting networks of lines. Int. J. Comp. Vis. **43** (2001) 99–111
2. Cohen, L., Kimmel, R.: Global minimum for active contour models: a minimal path approach. Int. J. Comp. Vis. **24** (1997) 57–78
3. Shackelford, A., Davis, C.: Fully automated road network extraction from high-resolution satellite multispectral imagery. In: Proc. IGARSS. Volume 1. (2003) 461–463
4. Soille, P., Grazzini, J.: Extraction of river networks from satellite images by combining mathematical morphology and hydrology. In: Proc. CAIP. Volume 4673 of LNCS. Springer-Verlag (2007) 636–644

5. Ichoku, C., Karnieli, A., Meisels, A., Chorowicz, J.: Detection of drainage channel networks on digital satellite images. Int. J. Rem. Sens. **17** (1996) 1659–1678
6. Baumgartner, A., Steger, C., Mayer, H., Echstein, W., Ebner, H.: Automatic road extraction based on multi-scale, grouping, and context. Photo. Eng. Rem. Sens. **65** (1999) 777–785
7. Barzohar, M., Cooper, D.: Automatic finding of main roads in aerial images by using geometric stochastic models and estimation. IEEE Trans. Patt. Ana. Mach. Intell. **18** (1996) 707–721
8. Hoover, A., Kouznetsova, V., Goldbaum, M.: Locating blood vessels in retinal images by piecewise threshold probing of a matched filter response. IEEE Trans. Med. Im. **19** (2000) 203–210
9. Dillabaugh, C., Niemann, K., Richardson, D.: Semi-automated extraction of rivers from digital imagery. GeoInform. **6** (2002) 263–284
10. Lecornu, L., Jacq, J.J., Roux, C.: Simultaneous tracking of the two edges of linear structures. In: Proc. IEEE ICIP. (1994) 188–192
11. Benmansour, F., Cohen, L.: Fast object segmentation by growing minimal paths from a single point on 2D or 3D images. J. Math. Vis. **33** (2009) 209–221
12. Péchaud, M., Keriven, R., Peyré, G.: Extraction of tubular structures over an orientation domain. In: Proc. IEEE CVPR. (2009) 336–342
13. Steger, C.: An unbiased detector of curvilinear structures. IEEE Trans. Patt Ana. Mach. Intell. **20** (1998) 113–125
14. Zlotnick, A., Carnine, P.: Finding road seeds in aerial images. Comp. Vis. Graph. Im. Proc. **57** (1993) 243–260
15. Merlet, N., Zerubia, J.: New prospects in line detection by dynamic programming. IEEE Trans. Patt. Ana. Mach. Intell. **18** (1996) 426–431
16. Peyré, G., Cohen, L.: Geodesic methods for shape and surface processing. In Tavares, J., Jorge, R., eds.: Advances in Computational Vision and Medical Image Processing: Methods and Applications. Volume 13 of Computational Methods in Applied Sciences. Springer (2009) 29–56
17. Soille, P., Talbot, H.: Directional morphological filtering. IEEE Trans. Patt. Ana. Mach. Intell. **23** (2001) 1313–1329
18. Soille, P.: On morphological operators based on rank filters. Patt. Recog. **35** (2002) 527–535
19. Ikonen, L., Toivanen, P.: Distance and nearest neighbor transforms on gray-level surfaces. Patt. Recog. Lett. **28** (2007) 604–612
20. Kimmel, R., Sethian, J.: Computing geodesic paths on manifolds. Proc. Nat. Aca. Sci. **95** (1998) 8431–8435
21. Köthe, U.: Integrated edge and junction detection with the boundary tensor. In: Proc. ICCV. (2003) 424–431
22. Prados, E., Lenglet, C., Pons, J., Wotawa, N., Deriche, R., Faugeras, O., Soatto, S.: Control theory and fast marching methods for brain connectivity mapping. In: Proc. IEEE CVPR. (2006) 1076–1083
23. Colombo, R., Vogt, J., Soille, P., Paracchini, M., de Jager, A.: Deriving river networks and catchments at the european scale from medium resolution digital elevation data. Cat. **70** (2007) 296–305
24. Paik, K.: Global search algorithm for nondispersive flow path extraction. J. Geo. Res. **113** (2008) F04001
25. Berntson, G.: The characterization of topology: a comparison of four topological indices for rooted binary trees. J. Theo. Bio. **177** (1995) 271–281